Optical waveguides

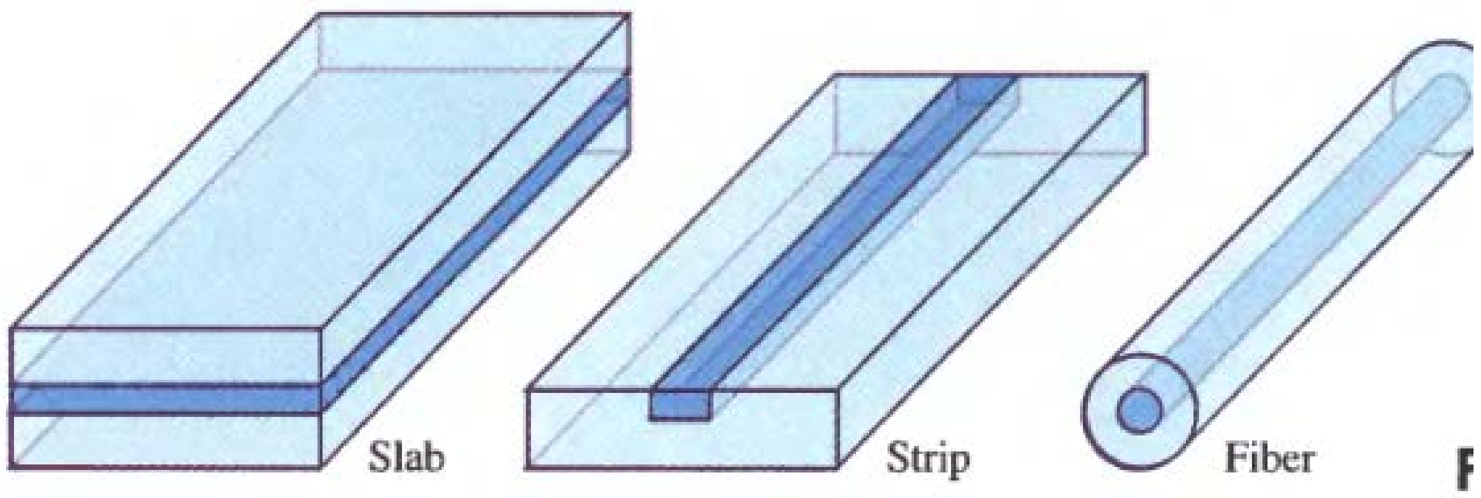

Planar-mirror waveguide

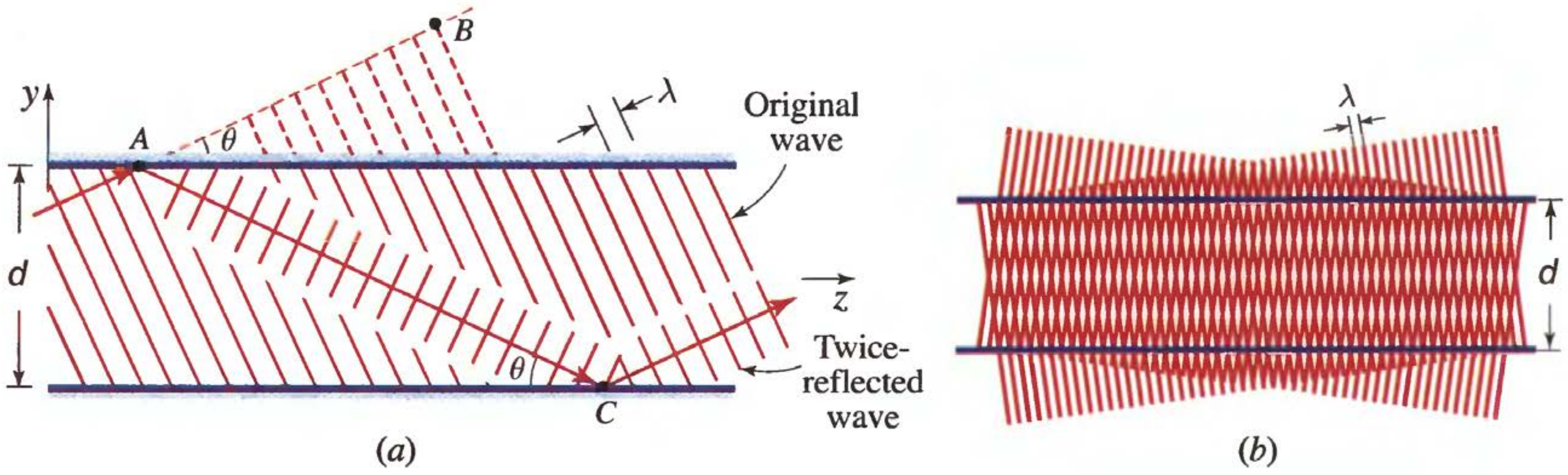

Figure 8.1-2 (*a*) Condition of self-consistency: as a wave reflects twice it duplicates itself. (*b*) At angles for which self-consistency is satisfied, the two waves interfere and create a pattern that does not change with z.

$$\Delta\varphi = 2\pi\overline{AC}/\lambda - 2\pi - 2\pi\overline{AB}/\lambda = 2\pi q$$

$$\sin\theta_m = m\,\frac{\lambda}{2d}, \qquad m = 1, 2, \ldots.$$

$$\beta \equiv k_z = k\cos\theta. \qquad \beta_m^2 = k^2 - \frac{m^2\pi^2}{d^2}.$$

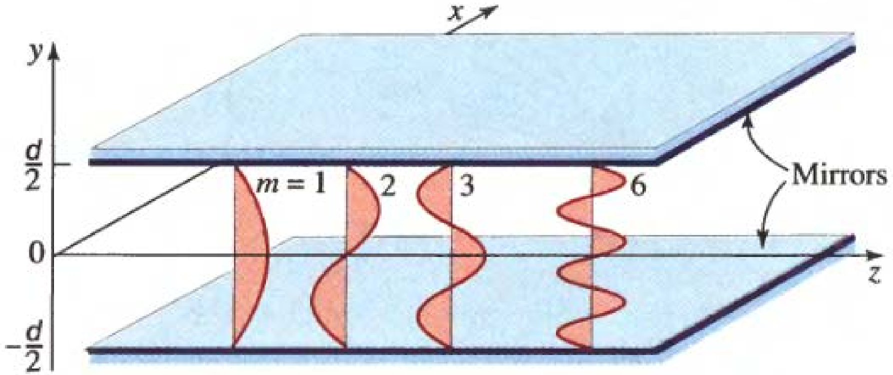

Figure 8.1-4 Field distributions of the modes of a planar-mirror waveguide.

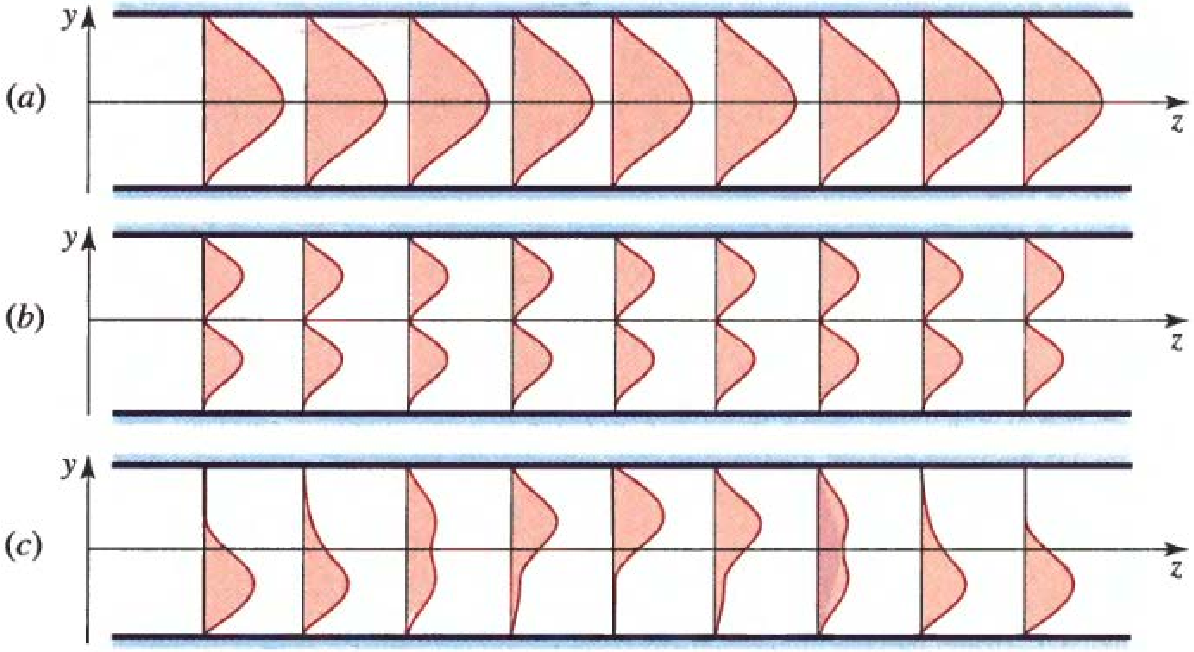

Figure 8.1-8 Variation of the intensity distribution in the transverse direction y at different axial distances z. (a) The electric-field complex amplitude in mode 1 is $E(y,z) = u_1(y)\exp(-j\beta_1 z)$, where $u_1(y) = \sqrt{2/d}\cos(\pi y/d)$. The intensity does not vary with z. (b) The complex amplitude in mode 2 is $E(y,z) = u_2(y)\exp(-j\beta_2 z)$, where $u_2(y) = \sqrt{2/d}\sin(2\pi y/d)$. The intensity does not vary with z. (c) The complex amplitude in a mixture of modes 1 and 2, $E(y,z) = u_1(y)\exp(-j\beta_1 z) + u_2(y)\exp(-j\beta_2 z)$. Since $\beta_1 \neq \beta_2$, the intensity distribution changes with z.

This relation may be written in terms of the cutoff angular frequency $\omega_c = 2\pi\nu_c = \pi c/d$ as

$$\beta_m = \frac{\omega}{c}\sqrt{1 - m^2\frac{\omega_c^2}{\omega^2}}. \tag{8.1-12}$$

Dispersion Relation

As shown in Fig. 8.1-5(*b*) for $m = 1, 2, \ldots$, the propagation constant β for mode m is zero at angular frequency $\omega = m\omega_c$, increases monotonically with angular frequency, and ultimately approaches the linear relation $\beta = \omega/c$ for sufficiently large values of β.

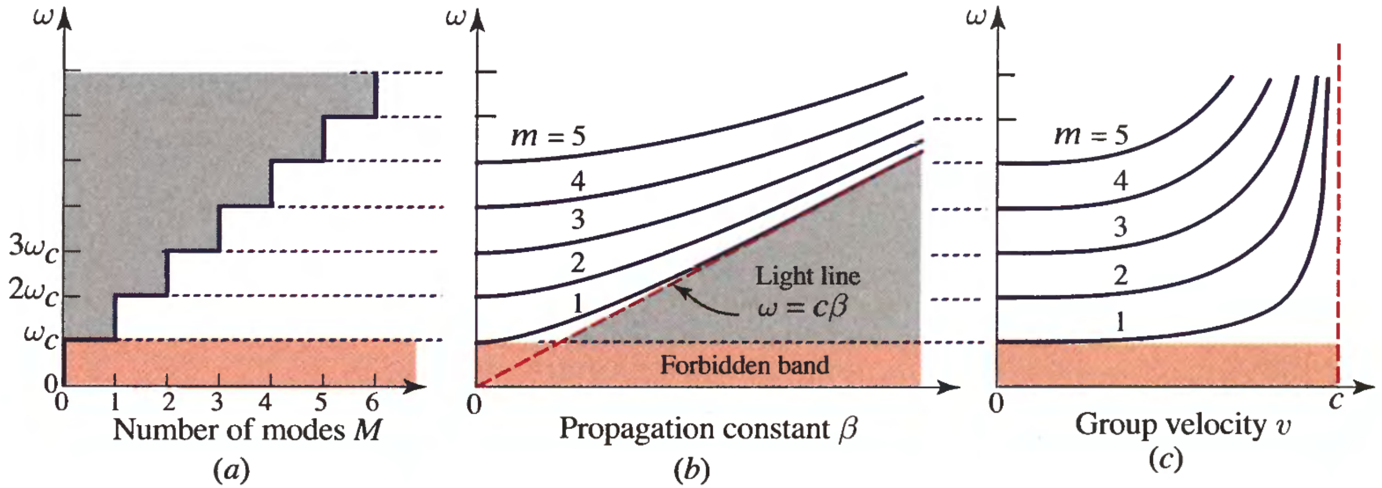

Figure 8.1-5 (*a*) Number of modes M as a function of angular frequency ω. Modes are not permitted for angular frequencies below the cutoff, $\omega_c = \pi c/d$. M increments by unity as ω increases by ω_c. (*b*) Dispersion relation. A forbidden band exists for angular frequencies below ω_c. (*c*) Group velocities of the modes as a function of angular frequency.

Planar-dielectric waveguide

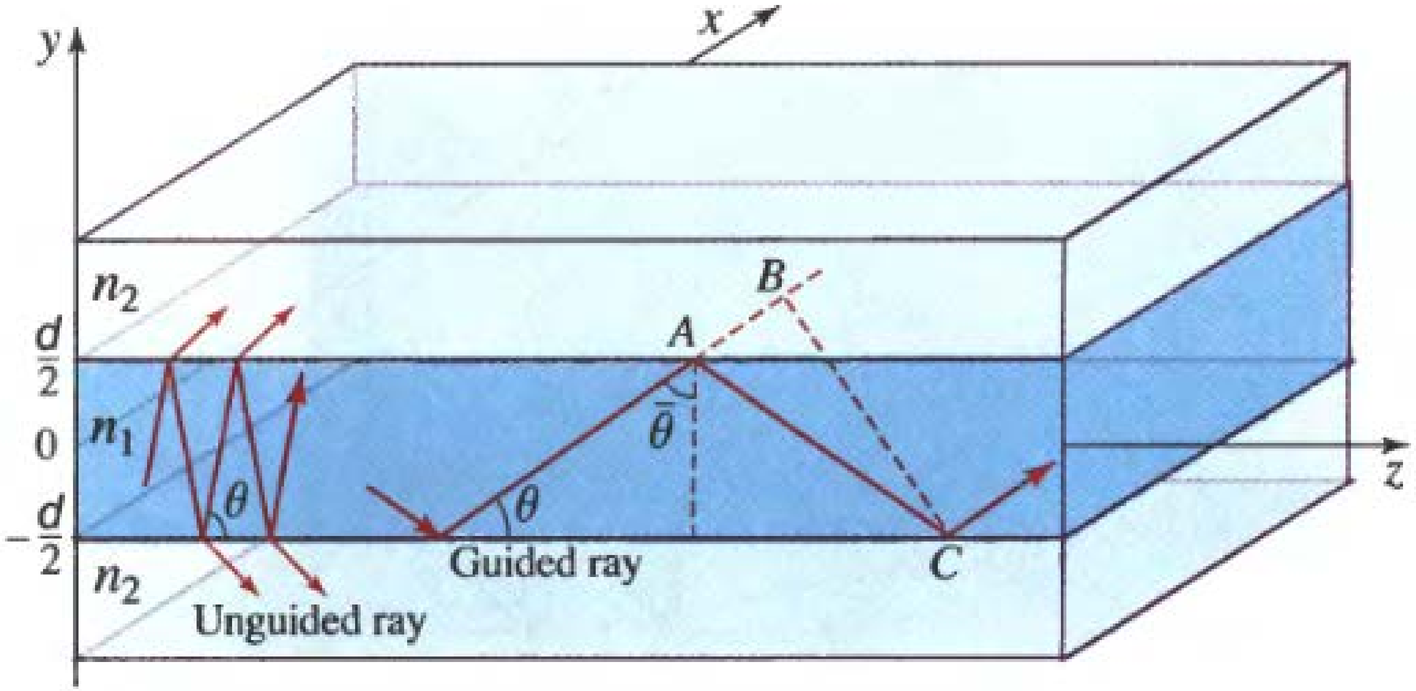

Figure 8.2-1 Planar dielectric (slab) waveguide. Rays making an angle $\theta < \bar{\theta}_c = \cos^{-1}(n_2/n_1)$ are guided by total internal reflection.

$$\frac{2\pi}{\lambda} 2d \sin\theta - 2\varphi_r = 2\pi m, \qquad m = 0, 1, 2, \ldots$$

$\theta_1 = \pi/2 - \theta$ and $\theta_c = \pi/2 - \bar{\theta}_c$ in (6.2-11)

$$\tan\frac{\varphi_r}{2} = \sqrt{\frac{\sin^2\bar{\theta}_c}{\sin^2\theta} - 1},$$

$$2k_y d - 2\varphi_r = 2\pi m.$$

so that φ_r varies from π to 0 as θ varies from 0 to $\bar{\theta}_c$. Rewriting (8.2-1) in the form $\tan(\pi d \sin\theta/\lambda - m\pi/2) = \tan(\varphi_r/2)$ and using (8.2-3), we obtain

$$\tan\left(\pi \frac{d}{\lambda}\sin\theta - m\frac{\pi}{2}\right) = \sqrt{\frac{\sin^2\bar{\theta}_c}{\sin^2\theta} - 1}\,. \qquad (8.2\text{-}4)$$

Self-Consistency Condition (TE Modes)

Compare with planar-mirror case:

$$\sin\theta_m = m\frac{\lambda}{2d}, \qquad m = 1, 2, \ldots$$

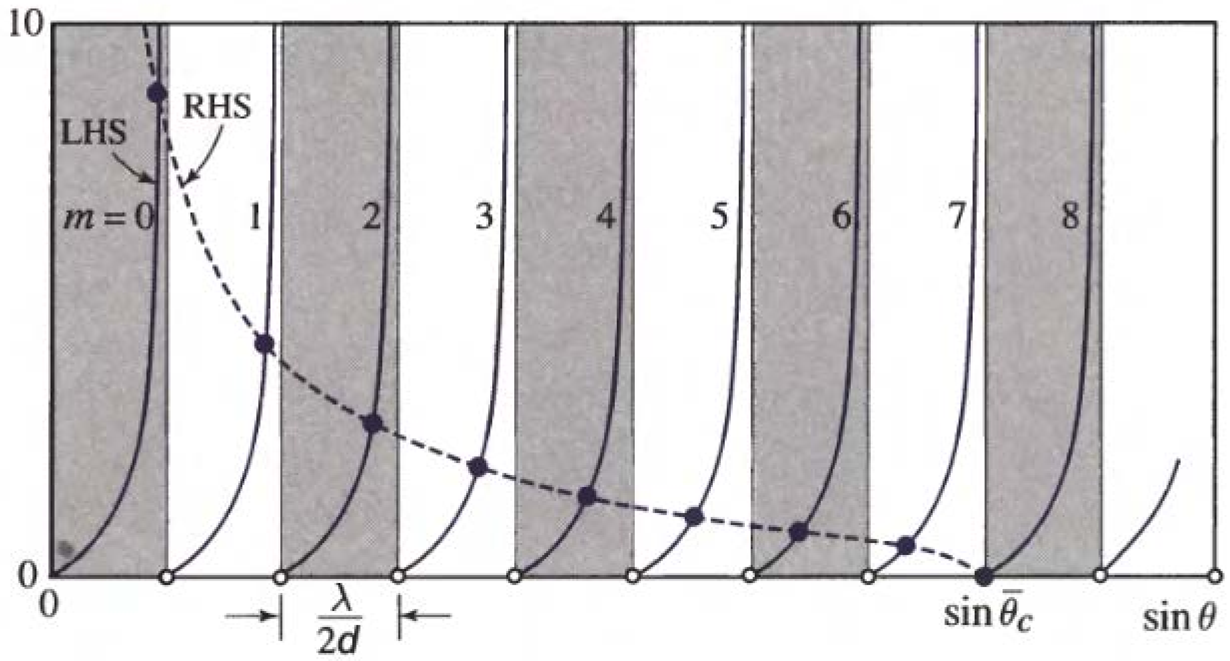

Figure 8.2-2 Graphical solution of (8.2-4) to determine the bounce angles θ_m of the modes of a planar dielectric waveguide. The RHS and LHS of (8.2-4) are plotted versus $\sin\theta$. The intersection points, marked by filled circles, determine $\sin\theta_m$. Each branch of the tan or cot function in the LHS corresponds to a mode. In this plot $\sin\bar{\theta}_c = 8(\lambda/2d)$ and the number of modes is $M = 9$. The open circles mark $\sin\theta_m = m\lambda/2d$, which provide the bounce angles of the modes of a planar-mirror waveguide of the same dimensions.

"Internal" solution:

$$u_m(y) \propto \begin{cases} \cos\left(2\pi \frac{\sin\theta_m}{\lambda} y\right), & m = 0, 2, 4, \ldots \\ \sin\left(2\pi \frac{\sin\theta_m}{\lambda} y\right), & m = 1, 3, 5, \ldots, \end{cases} \qquad -\frac{d}{2} \le y \le \frac{d}{2},$$

"External" solution, match at boundaries (homework):

$$u_m(y) \propto \begin{cases} \exp(-\gamma_m y), & y > d/2 \\ \exp(\gamma_m y), & y < -d/2. \end{cases}$$

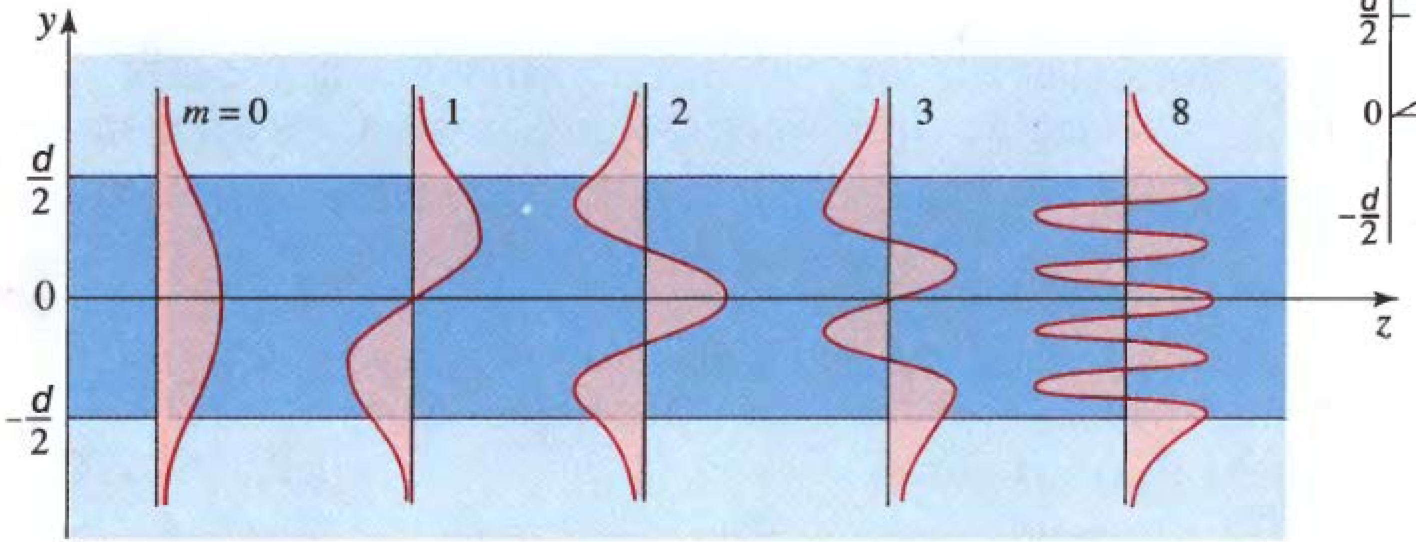

Compare with planar-mirror case:

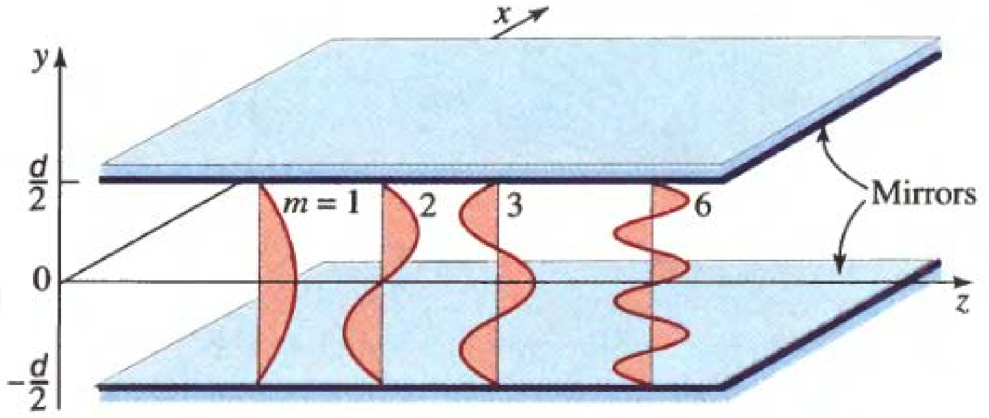

Figure 8.2-5 Field distributions for TE guided modes in a dielectric waveguide. These results should be compared with those shown in Fig. 8.1-4 for the planar-mirror waveguide.

Two-dimensional waveguides

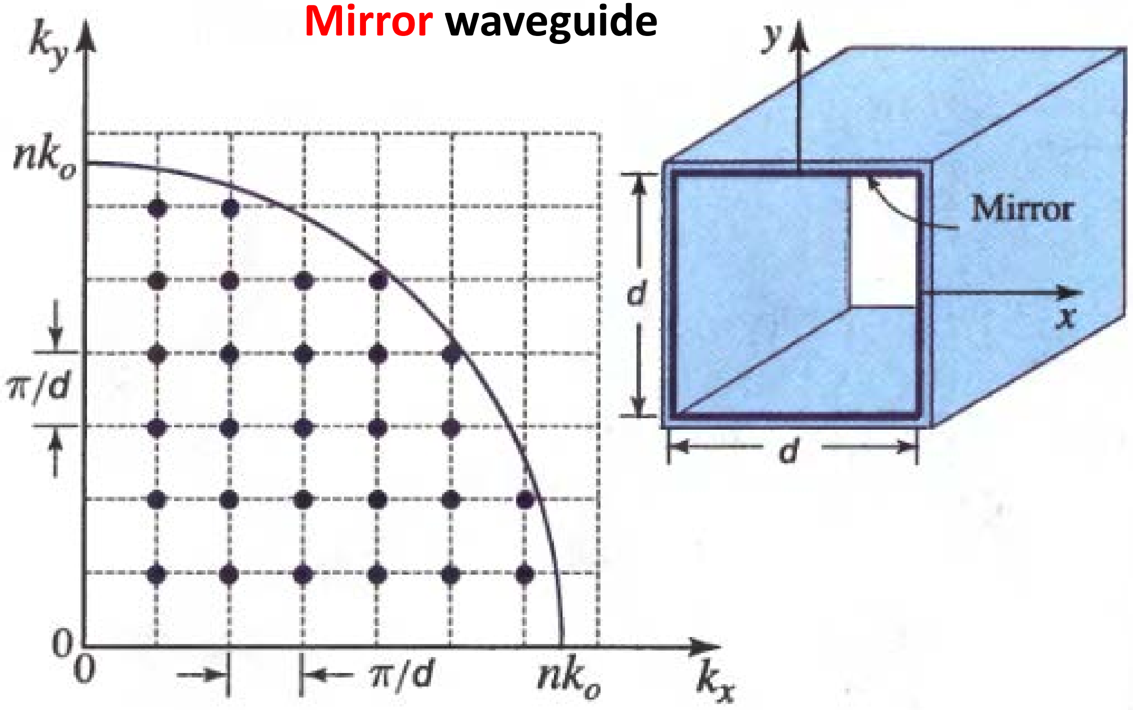

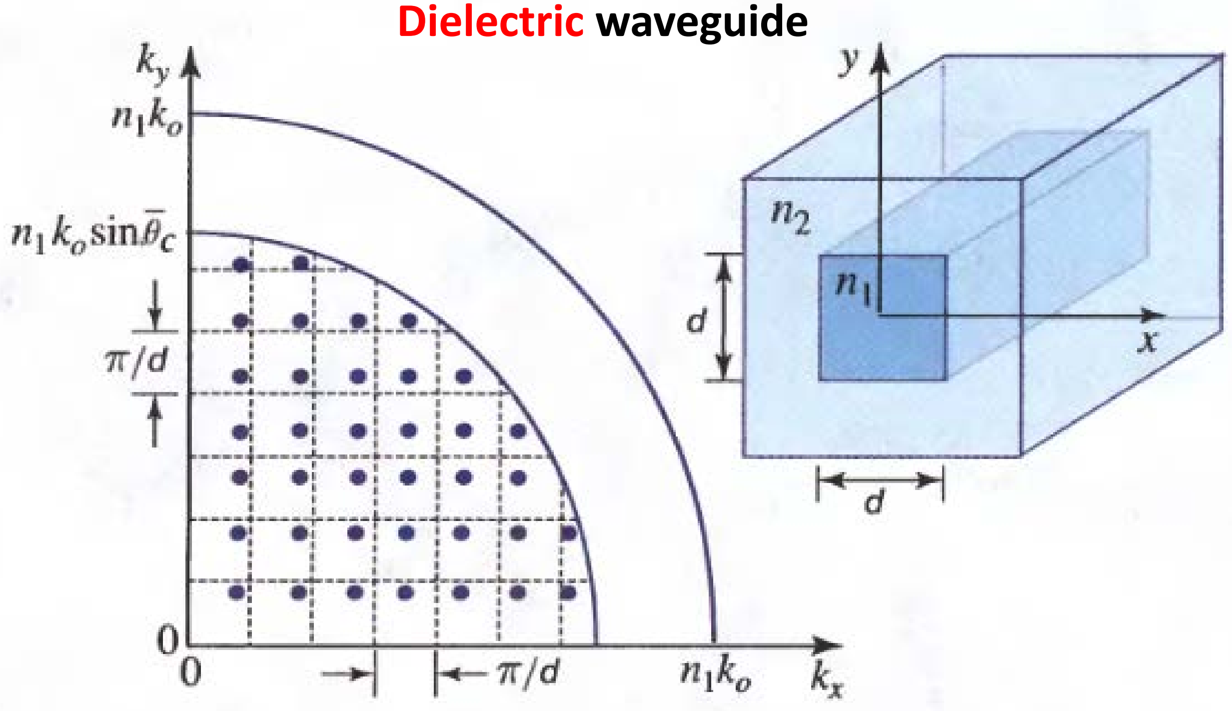

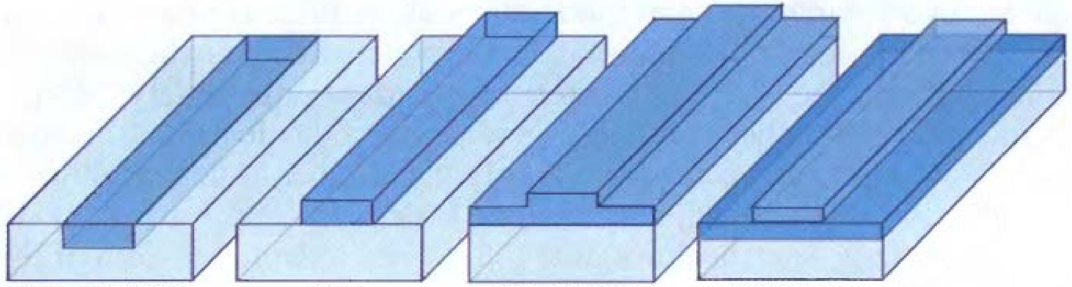

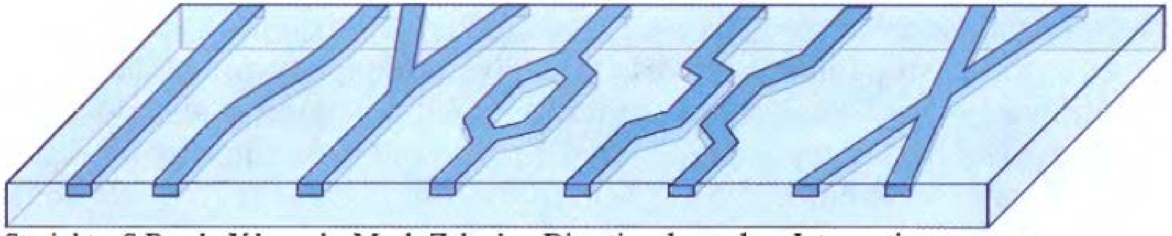

Figure 8.3-3 Various waveguide geometries. The darker the shading, the higher the refractive index.

Photonic crystal waveguides

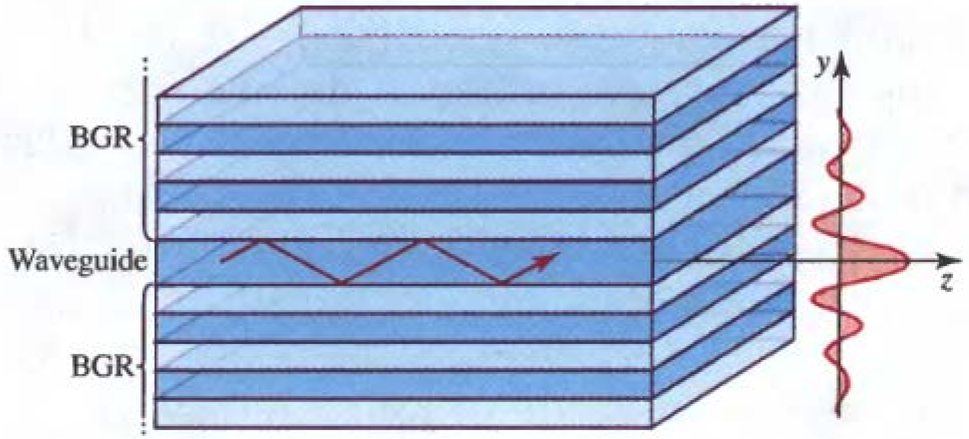

Figure 8.4-1 Planar waveguide made of a dielectric slab sandwiched between two Bragg-grating reflectors (BGR).

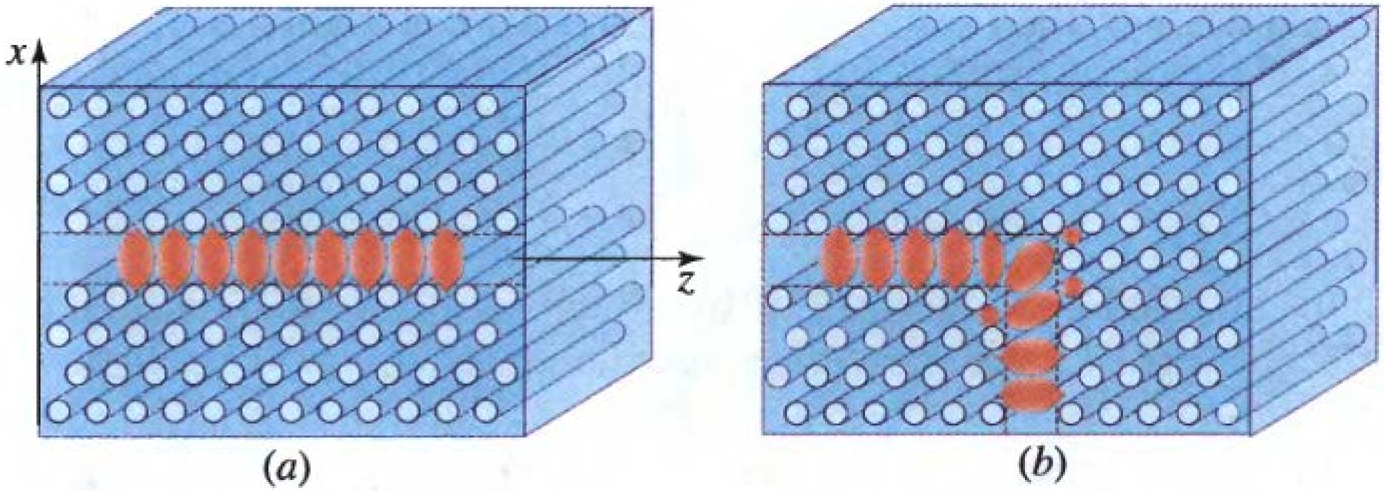

Figure 8.4-3 (*a*) Propagating mode in a photonic-crystal waveguide. (*b*) L-shaped photonic-crystal waveguide.

Fiber optics

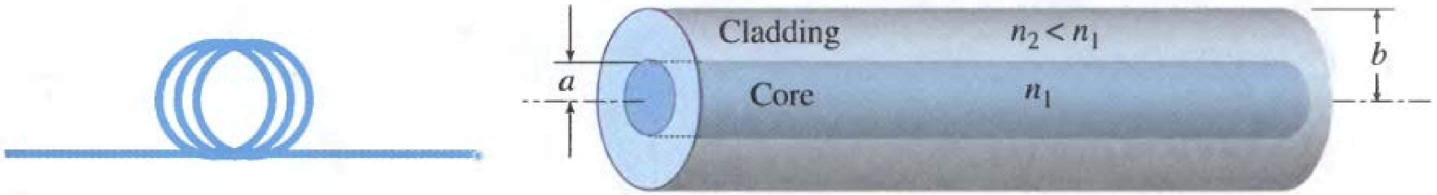

Figure 9.0-1 An optical fiber is a cylindrical dielectric waveguide with an inner core and an outer cladding.

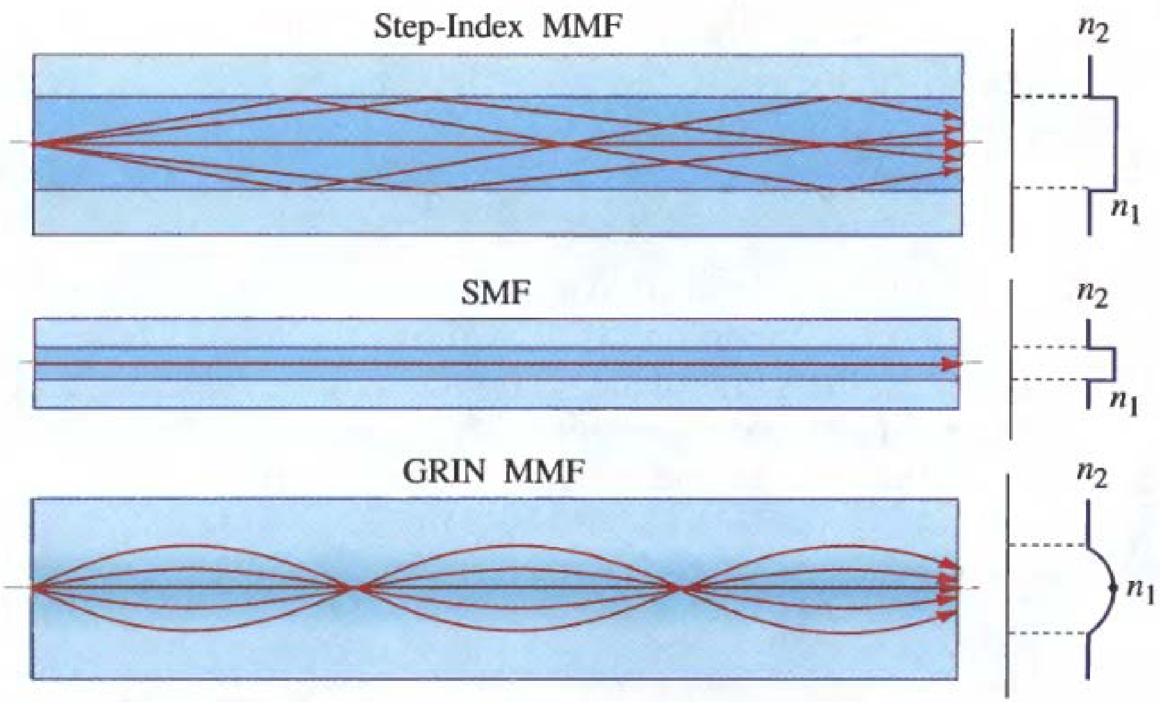

Figure 9.0-2 Geometry, refractive-index profile, and typical rays in a step-index multimode fiber (MMF), a single-mode fiber (SMF), and a graded-index multimode fiber (GRIN MMF).

Fiber optics as **guided rays**

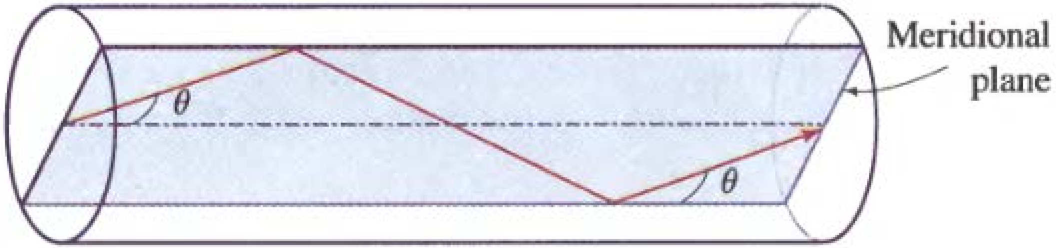

Figure 9.1-1 The trajectory of a meridional ray lies in a plane that passes through the fiber axis. The ray is guided if $\theta < \bar{\theta}_c = \cos^{-1}(n_2/n_1)$.

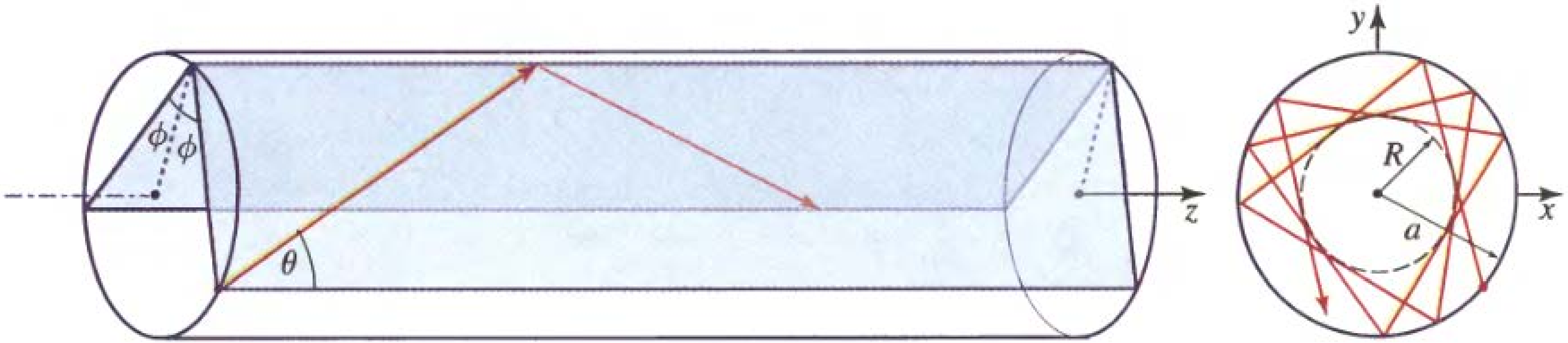

Figure 9.1-2 A skewed ray lies in a plane offset from the fiber axis by a distance R. The ray is identified by the angles θ and ϕ. It follows a helical trajectory confined within a cylindrical shell with inner and outer radii R and a, respectively. The projection of the ray on the transverse plane is a regular polygon that is not necessarily closed.

Fiber optics as guided rays

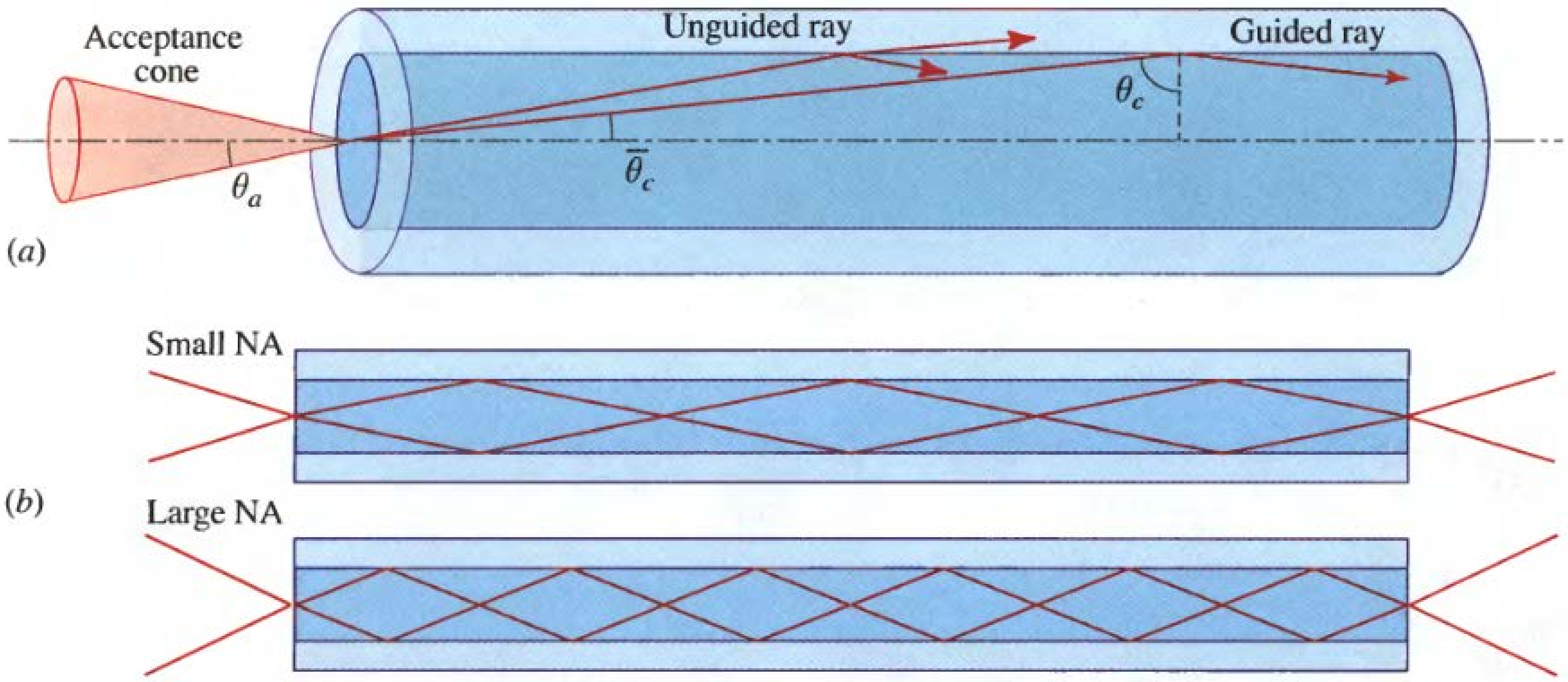

Figure 9.1-3 (*a*) The acceptance angle θ_a of a fiber. Rays within the acceptance cone are guided by total internal reflection. The numerical aperture NA $= \sin\theta_a$. The angles θ_a and $\bar{\theta}_c$ are typically quite small; they are exaggerated here for clarity. (*b*) The light-gathering capacity of a large NA fiber is greater than that of a small NA fiber.

Fiber optics as guided WAVES

$$u(r) \propto \begin{cases} J_l(k_T r), & r < a \quad \text{(core)} \\ K_l(\gamma r), & r > a \quad \text{(cladding)}, \end{cases}$$

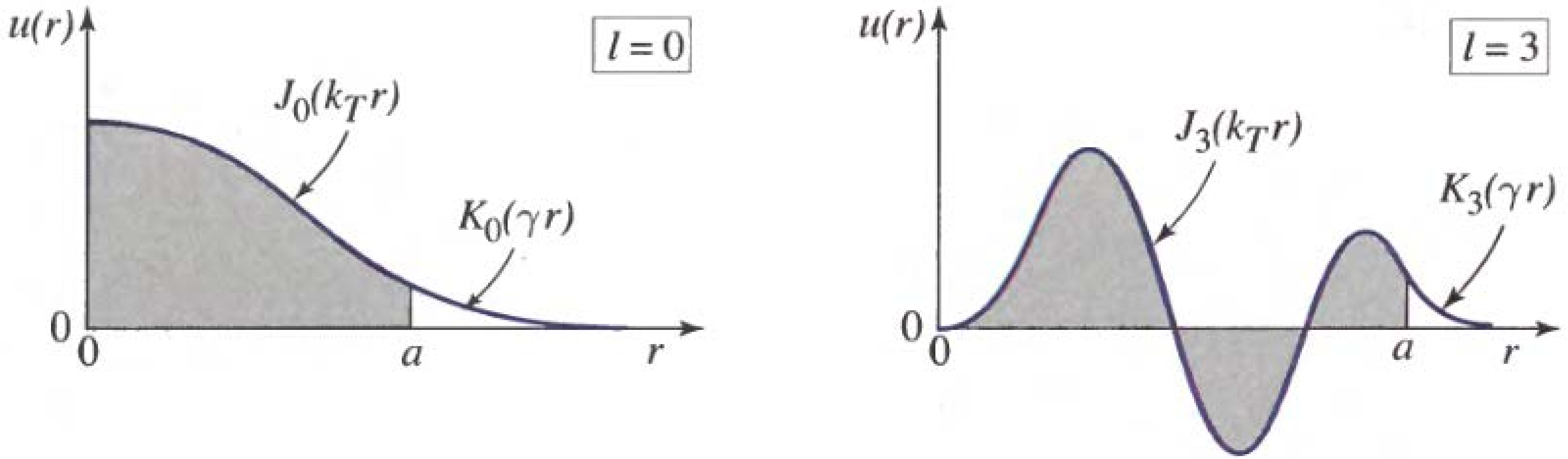

Figure 9.2-2 Examples of the radial distribution $u(r)$ provided in (9.2-6) for $l = 0$ and $l = 3$. The shaded and unshaded areas represent the fiber core and cladding, respectively. The parameters k_T and γ, and the two proportionality constants in (9.2-6), have been selected such that $u(r)$ is continuous and has a continuous derivative at $r = a$. Larger values of k_T and γ lead to a greater number of oscillations in $u(r)$.

Similar to the planar (& 2D) dielectric waveguide solutions:

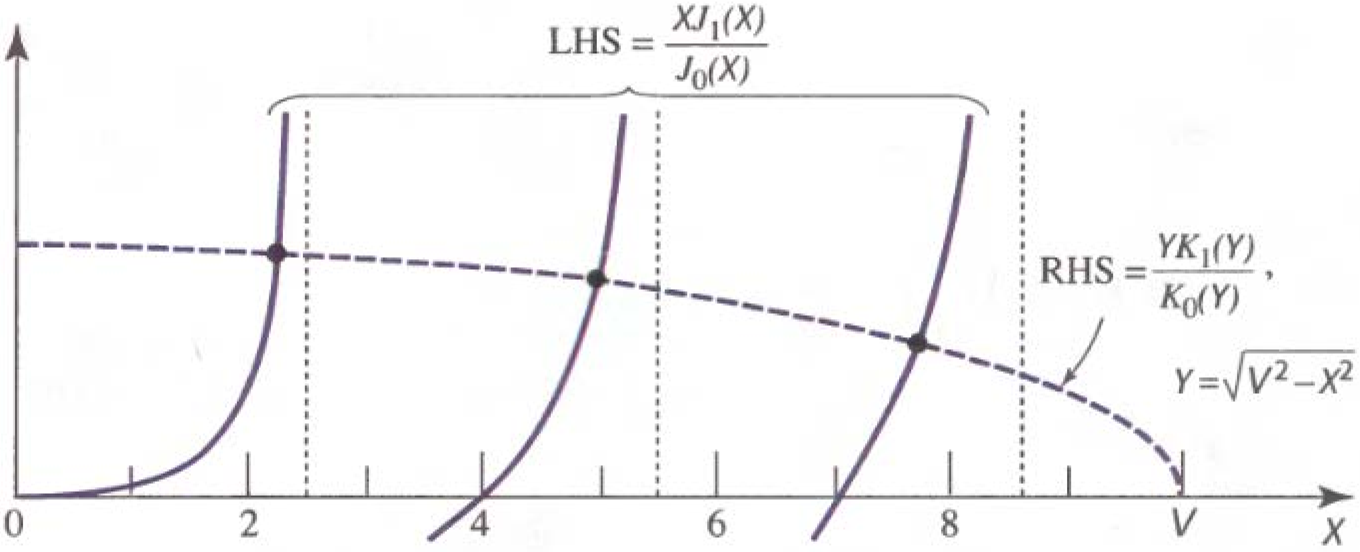

Figure 9.2-3 Graphical construction for solving the characteristic equation (9.2-14). The left- and right-hand sides are plotted as functions of X. The intersection points are the solutions. The LHS has multiple branches intersecting the abscissa at the roots of $J_{l\pm1}(X)$. The RHS intersects each branch once and meets the abscissa at $X = V$. The number of modes therefore equals the number of roots of $J_{l\pm1}(X)$ that are smaller than V. In this plot $l = 0$, $V = 10$, and either the $-$ or $+$ signs in (9.2-14) may be used.

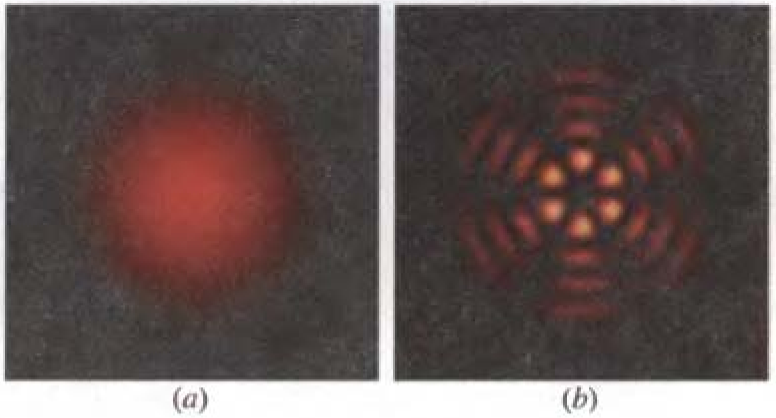

Figure 9.2-4 Intensity distributions of (*a*) the LP_{01} and (*b*) the LP_{34} modes in the transverse plane, assuming an azimuthal dependence of the form $\cos l\phi$. The distribution of the fundamental LP_{01} mode is similar to that of the Gaussian beam discussed in Chapter 3.

Polarization maintaining fibers

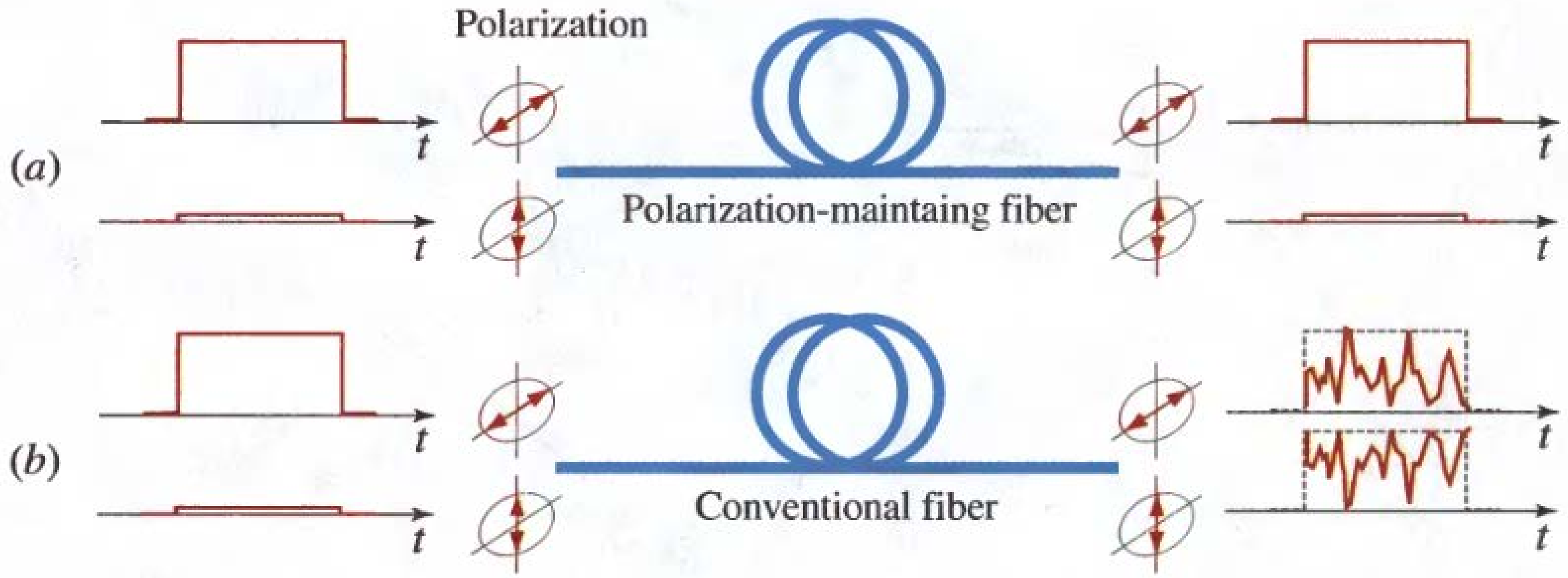

Figure 9.2-9 (*a*) Ideal polarization-maintaining fiber. (*b*) Random transfer of power between two polarizations.

Why telecom uses 1550 nm light:

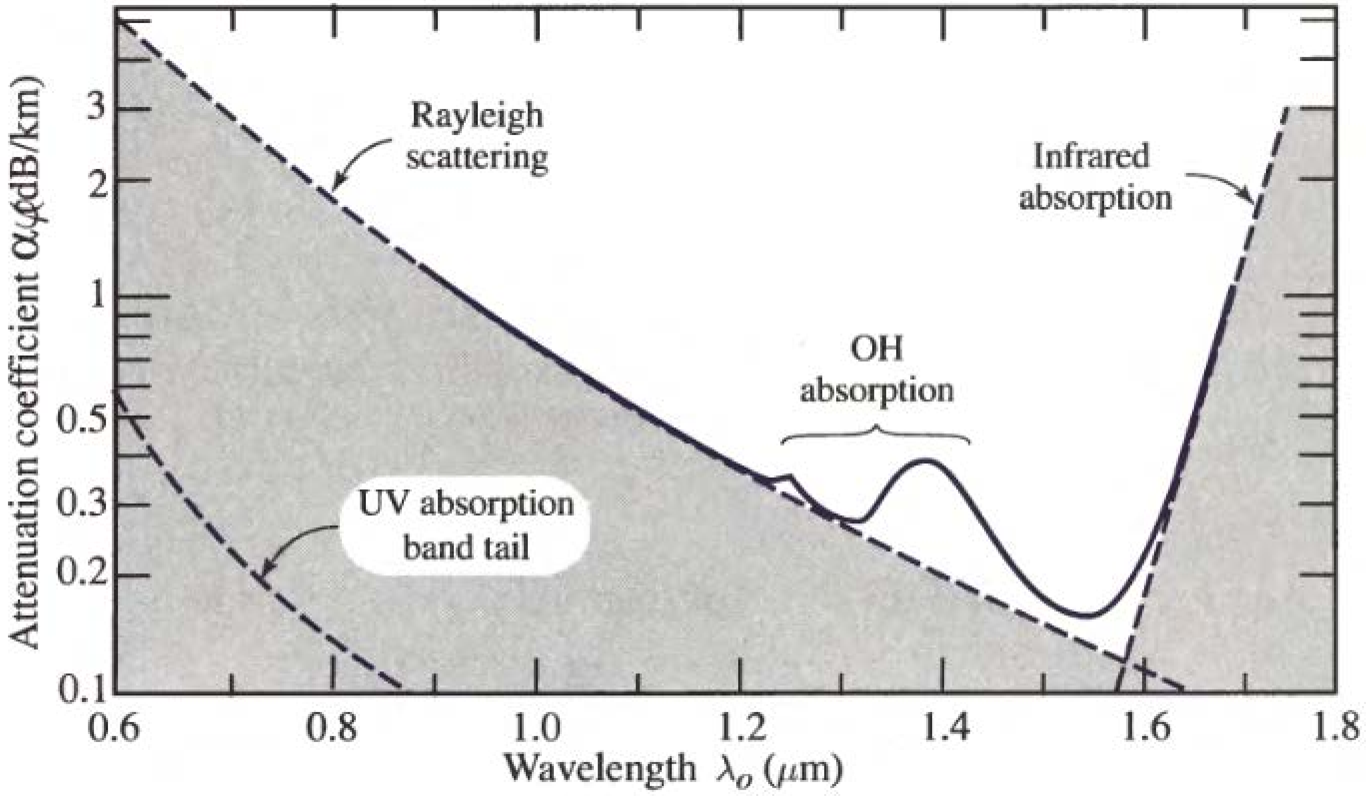

Figure 9.3-2 Attenuation coefficient α of silica glass versus wavelength λ_o. There is a local minimum at 1.3 μm ($\alpha \approx 0.3$ dB/km) and an absolute minimum at 1.55 μm ($\alpha \approx 0.15$ dB/km).

Finally, the ultimate fiber: Photonic crystal fibers

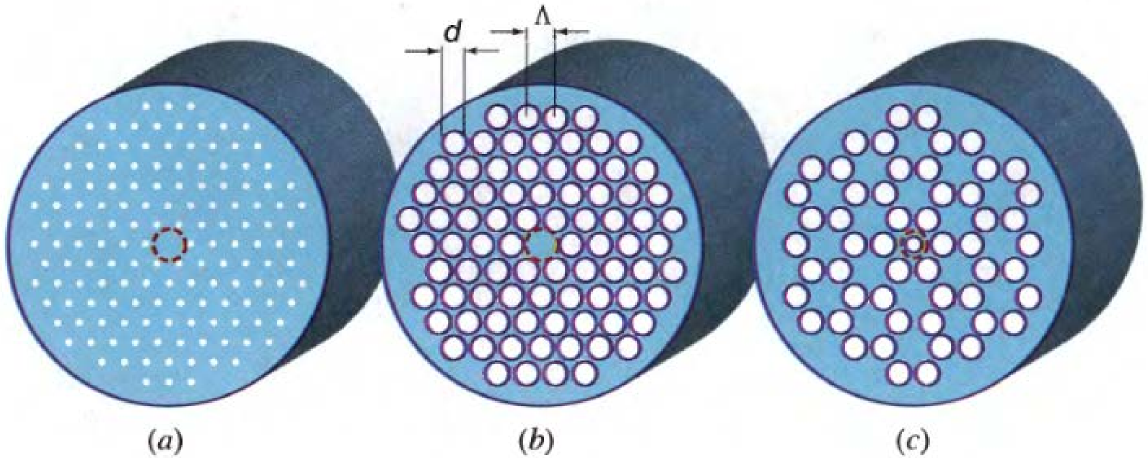

Figure 9.4-1 Various forms of holey fibers. (*a*) Solid core (dotted circle) surrounded by a cladding of the same material but suffused with a periodic array of cylindrical air holes whose diameters are much smaller than a wavelength. The average refractive index of the cladding is lower than that of the core. (*b*) Photonic-crystal holey fiber with cladding that contains a periodic array of large air holes and a solid core (dotted circle). (*c*) Photonic-crystal holey fiber with cladding that contains a periodic array of large air holes and a core that is an air hole of a different size (dotted circle).

Benefits:

- Single mode for a broad range of wavelengths
- Large mode area, e.g., step-index fiber 5 um, vs 50 um
- -> can handle more power
- Dispersion can also be engineered

Goos–Hänchen Shift. Consider two TE plane waves undergoing total internal reflection at angles θ and $\theta + d\theta$, where $d\theta$ is an incremental angle. If the phase retardation introduced between the reflected waves is written in the form $d\varphi = \xi \, d\theta$, find an expression for the coefficient ξ. Sketch the interference patterns of the two incident waves and the two reflected waves and verify that they are shifted by a lateral distance proportional to ξ. When the incident wave is a beam (composed of many plane-wave components), the reflected beam is displaced laterally by a distance proportional to ξ. This is known as the Goos–Hänchen effect.